Journal of the Mechanics and Physics of Solids 59 (2011) 595–609

Contents lists available at ScienceDirect

Journal of the Mechanics and Physics of Solids

journal homepage: www.elsevier.com/locate/jmps

An energy-based microstructure model to account for fatigue scatter in polycrystals

Michael D. Sangid [a,*], Hans J. Maier [b], Huseyin Sehitoglu [a]

[a] Department of Mechanical Science and Engineering, University of Illinois at Urbana-Champaign, 1206 W. Green St., Urbana, IL 61801, USA
[b] Lehrstuhl für Werkstoffkunde (Materials Science), University of Paderborn, 33095 Paderborn, Germany

ARTICLE INFO

Article history:
Received 8 July 2010
Received in revised form
28 October 2010
Accepted 19 December 2010
Available online 4 January 2011

Keywords:
Fatigue crack initiation—life prediction
Grain boundaries
Microstructures
Polycrystalline material
Energy methods
Scatter

ABSTRACT

Scatter observed in the fatigue response of a nickel-based superalloy, U720, is linked to the variability in the microstructure. Our approach is to model the energy of a persistent slip band (PSB) structure and use its stability with respect to dislocation motion as our failure criterion for fatigue crack initiation. The components that contribute to the energy of the PSB are identified, namely, the stress field resulting from the applied external forces, dislocation pile-ups, and work-hardening of the material is calculated at the continuum scale. Further, energies for dislocations creating slip in the matrix/precipitates, interacting with the GBs, and nucleating/agglomerating within the PSB are computed via molecular dynamics simulations. Through this methodology, fatigue life is predicted based on the energy of the PSB, which inherently accounts for the microstructure of the material. The present approach circumvents the introduction of uncertainty principles in material properties. It builds a framework based on mechanics of microstructure, and from this framework, we construct simulated microstructures based on the measured distributions of grain size, orientation, neighbor information, and grain boundary character, which allows us to calculate fatigue scatter using a deterministic approach. The uniqueness of the approach is that it avoids the large number of parameters prevalent in previous fatigue models. The predicted lives are in excellent agreement with the experimental data validating the model capabilities.

1. Introduction

There exists inherent variability in every material property due to: inhomogeneity in the material at the microstructure level, differences between heats and vendors, allowable ranges in the chemical compositions, the response of various impurities, stochastic mechanical behavior, testing differences, etc. This material variability is even more pronounced when viewing the fatigue response of a material. In the high cycle regime (the material undergoes primarily elastic loading), the fatigue life is dominated by the initiation and growth of a single crack, thus deviation in the probability of failure is a function of applied stress/strain (Pineau, 2001). As opposed to the low cycle regime (loads are sufficient to yield the material during each cycle) where multiple cracks initiate and interact with one another, the fatigue scatter is a

* Corresponding author.
E-mail addresses: msangid@illinois.edu (M.D. Sangid), huseyin@illinois.edu (H. Sehitoglu).

0022-5096/$ - see front matter © 2010 Elsevier Ltd. All rights reserved.
doi:10.1016/j.jmps.2010.12.014

function of applied cycles. There have been many attempts made over the years to characterize the material variability through probabilistic models including statistical based and damage accumulation methods.

By use of statistical based methods, the log-normal fatigue and Weibull distributions are the most general and widely used model to fit fatigue scatter. For each applied stress or strain range, a distribution of failure is calculated (Suresh, 1998). Further, Socie argued that the standard empirically based Coffin–Manson model should be generalized to account for the probabilistic response of the curve fit parameters (Socie, 2005) to capture the material variability in different life regimes. Using the response of a statistical model to simulate crack initiation, Provan and Ghonem account for variability in strength characteristics of a polycrystalline material to applied load, residual stresses, work hardening, and the accumulation of damage (Ghonem and Provan, 1980); although this model does not account for variability in the microstructure such as grain size, orientation, or misorientation. It is known that the grain size has a first order affect on fatigue lives, although there are no current models that predict its role especially when a wide distribution of sizes can be present in the microstructure.

A subset of these statistical models is defect-based models, for materials whose primary failure mechanism are voids, inclusions, or second phase particles. Thus, finding the probability of cracks initiating from inclusions within a material has received a substantial amount of attention over the years (Grison and Remy, 1997; Pineau, 2001; Todinov, 1998). For these types of models, the information generated is valuable for forecasting failure, especially for materials which exhibit unimodal failure; although, the predicted values are only as useful as the accuracy of the input; thus, the size and spatial distribution of defects must be known a priori. In general, the difficulty in these statistical based models is that they require many tests to get a decent statistical representation of the material behavior. In these tests, the samples are treated as being identical to one another, thus these results are indifferent towards the failure mode or microstructural deviations within the material. These models, although valuable, are not designed to provide predictive capabilities in the presence of excessive scatter. Furthermore, with improvements in processing routes the source of crack initiation often could no longer be linked to distinct defects such as voids or inclusions, especially in superalloys.

Fatigue lives are dominated by damage formation, which is primarily driven by irreversible dislocation slip. Many damage accumulation models have been established, specifically in the form of stochastic crack propagation (Ellyin, 1986; Jeulin, 2001; Kulkarni et al., 2006; Wirsching et al., 1991). By accounting for grain boundaries (GBs), the results show that GBs resist slip and crack advancement resulting in damage preferentially accumulating along GBs (Kitamura et al., 1989; Qiao and Chakravarthula, 2005). Kato and Mori have made modifications to the well known Coffin–Manson and Palmgren–Miner empirical models to account for statistics based on the accumulation of completely irreversible damage. Their study show that the predicted fatigue lives become much longer when accounting for random stochastic damage (Kato and Mori, 1992). These types of analyses assume that microcracks are present in the material and are distributed according to a Poisson point process. This assumption has yet to be validated through experimental evidence. Further, the coalescence of these microcracks into a macrocrack in the case of multiple site damage is a stochastic process. It requires knowledge of the cracks spatial and size distributions in addition to knowledge about mechanisms in which they coalesce. This type of problem is very difficult and must be simplified by neglecting the local perturbations in the stress field induced by the cracks and the crack geometry (Pineau, 2001). Another potential problem in these models is the application and breakdown of linear elastic fracture mechanics to analyze short cracks with relatively large plastic zones ahead of the crack tips in comparison to the crack lengths.

The collection of probabilistic models used to account for fatigue scatter, as a whole, is missing certain aspects of the material behavior. In addition to this, the aforementioned models are not deterministic, since they do not clearly define a cause and effect rationale to predict failure, nor can they trace this failure back to the microstructural level. For instance, individual models have stated the important influence of GB effects, but these and other microstructural details need to be accounted for in each model. It is well known that the microstructure plays an essential role in fatigue crack initiation, such as grain size, grain orientation, and GB character (not only of a local grain but of its neighboring grains). In fact, one of the main factors controlling the lower limit of fatigue capabilities is the largest grain size within the microstructure (Miao et al., 2009). This type of information must be incorporated in these models to create a robust simulation for crack initiation.

One type of model that addresses the microstructures affect on the early fatigue response is presented by Przybyla and McDowell (2010), in which they apply a statistical framework to a cyclic crystal plasticity model. In doing so, they are able to determine a fatigue indicator parameter, which establishes the microstructure affect on the fatigue response of the polycrystalline aggregate. By use of a cyclic crystal plasticity approach, this method offers a physical understanding of failure, although it is extremely computationally intensive, thus, in its present form, it cannot be used to predict number of cycles to failure.

In this paper, we describe an approach to model the energy of a PSB structure and use its stability with respect to dislocation motion as our failure criterion for fatigue crack initiation. From this analysis, we are able to predict the fatigue life of polycrystalline specimens, which rely heavily on the microstructure of the material, namely grain orientations, widely distributed grain sizes, precipitates, GB characters, and the influence of neighboring grains. Once the microstructure characterization is established, we determine the distribution of individual crystallographic properties (such as grain size, Schmid factor, misorientation, and number of neighbors). Thus allowing us to simulate a microstructure for this material by randomly assigning microstructural attributes from these distributions, via a Monte Carlo approach. Hence the scatter and probability of failure are predicted from a deterministic approach, which is driven by the microstructure.

2. Material and experimental methods

The material utilized in this study is a Ni-based superalloy, Udimet 720 (U720). The primary strengthening mechanism in this material is in the form of ordered Ni_3Al-type precipitates ($L1_2$ structure), which occur in this material at three length scales (primary, secondary, and tertiary). The coherency of these γ' precipitate with respect to the γ matrix offers microstructural stability along with enhanced strengthening at elevated temperatures. The material underwent a solution process at 1100 °C for 2 h followed by oil quenching, in order to prepare the matrix for uniform precipitation of γ'. Afterwards, it was aged at 760 °C for 8 h with air-cooling, in order to precipitate the coarser γ', which offers creep resistance. A second aging process at 650 °C for 24 h with air-cooling produced fine γ' thus strengthening the microstructure for tensile and fatigue loads and stabilizing the γ' precipitates.

In this study, strain-controlled low cycle fatigue experiments were conducted on U720 specimens at three strain ranges (normalized values of 1.00%, 0.73%, and 0.69%, whereas each strain range is divided by the maximum tested strain range) at elevated temperature and R_ε=0. The resulting hysteresis response displays considerable plastic deformation during unloading and minimal ratcheting. Crack initiation was defined as the measured load amplitude dropping to a level of 90% of the saturated value. The fracture surface of the failed fatigue specimens were analyzed to study the mechanism for crack initiation, as shown in Fig. 1a,b. From Fig. 1a,b, twinning is observed near the facet features, thus indicating that cracks initiate near the twin boundaries, as reported in literature (Boettner et al., 1964; Guo et al., 2005; Hashimoto et al., 1999; Llanes and Laird, 1992; Miao et al., 2009; Qu et al., 2008; Thompson, 1972). Material characterization in the form of TEM analysis was performed, which provided key insights that can be used to model the microstructure and resulting dislocation arrangements. In the fatigued samples, slip and plastic strain are localized into banded regions. Fig. 1c shows a low-magnification TEM image of a persistent slip band in U720, and a more detailed view of two bands in this structure is shown in Fig. 1d. From this TEM analysis, we draw many insights into the strain localization that ultimately leads to failure within U720. Slip interacts with the grain boundary causing pile-up of dislocations and stress concentration, which results in slip penetrating into the second grain. By viewing the high magnification image, we see that the slip band forms by dislocations shearing the γ' precipitates resulting in slip being confined to a single glide plane (a 2D planar feature).

During the heat treatment process the γ' acts to pin the grain boundaries, thus determining the grain size in the γ matrix. In this material, there are areas of densely populated γ' alongside areas denuded of γ'. As a result, there exists a wide distribution of grain sizes, as fine grains form in regions of heavily populated γ' and coarse grains form in regions where γ' is sparse. Electron backscatter diffraction (EBSD) scans were completed on three samples: (1) fatigue specimen tested at the highest strain range, (2) fatigue specimen tested at the lowest strain range, and (3) an as-received specimen. The data from these three scans were pooled together, in order to find representative distributions of the grain size and orientations in terms of individual Schmid factors of the grains in the aggregate, as shown in Fig. 2a,b, respectively. The mean grain size is 3.4 μm, although the grain size distribution has a large tail indicating many larger grains are present, which results in a wide distribution of adjacent grains and GBs per grain (Fig. 2c). Further characterization on the GBs is necessary to understand their role in the fatigue response of the material, defined as the density of coincidental atoms between two lattices at the GB, where the density's reciprocal is denoted as the coincidental site lattice (CSL) Σ value. Hence, the CSL values of each GB is determined by the methodology described in Sangid et al. (2010) and shown in Fig. 2d. From these results, we see that fatigue testing did not significantly affect the texture or GB characters of the material.

The geometry of the PSB within the most favorably oriented grain of a polycrystal is shown in Fig. 3; from which, it can be seen that the dislocations localize into the PSB. The PSB intersects the GB; as a consequence of slip within the PSB. In

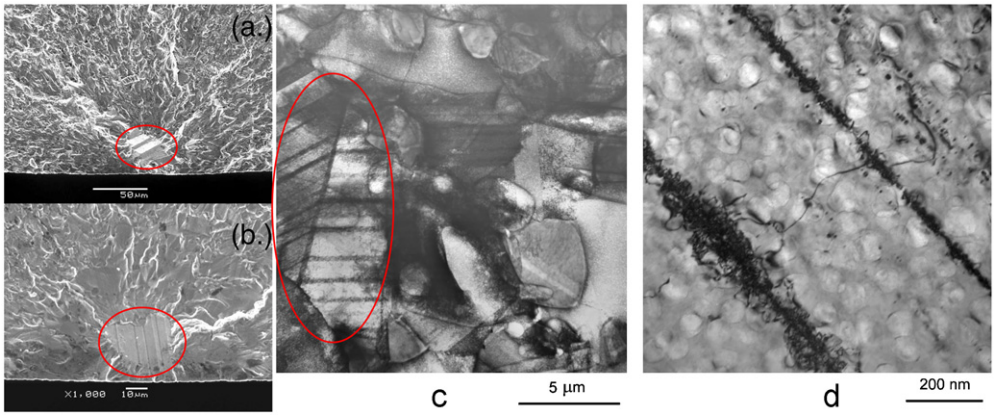

Fig. 1. (a, b) Fracture surface of a failed fatigue specimen, cracks initiate from facets, although considerable plasticity is involved in forming this feature. From the pictures, we can see evidence of twinning near the facets (c). A low-magnification TEM image of a persistent slip band (shown within the red ellipse). (d) A high-magnification image of two bands in a failed fatigue specimen of U720 tested at the highest strain range, R=0, and elevated temperature. (For interpretation of the references to color in this figure legend, the reader is referred to the web version of this article.)

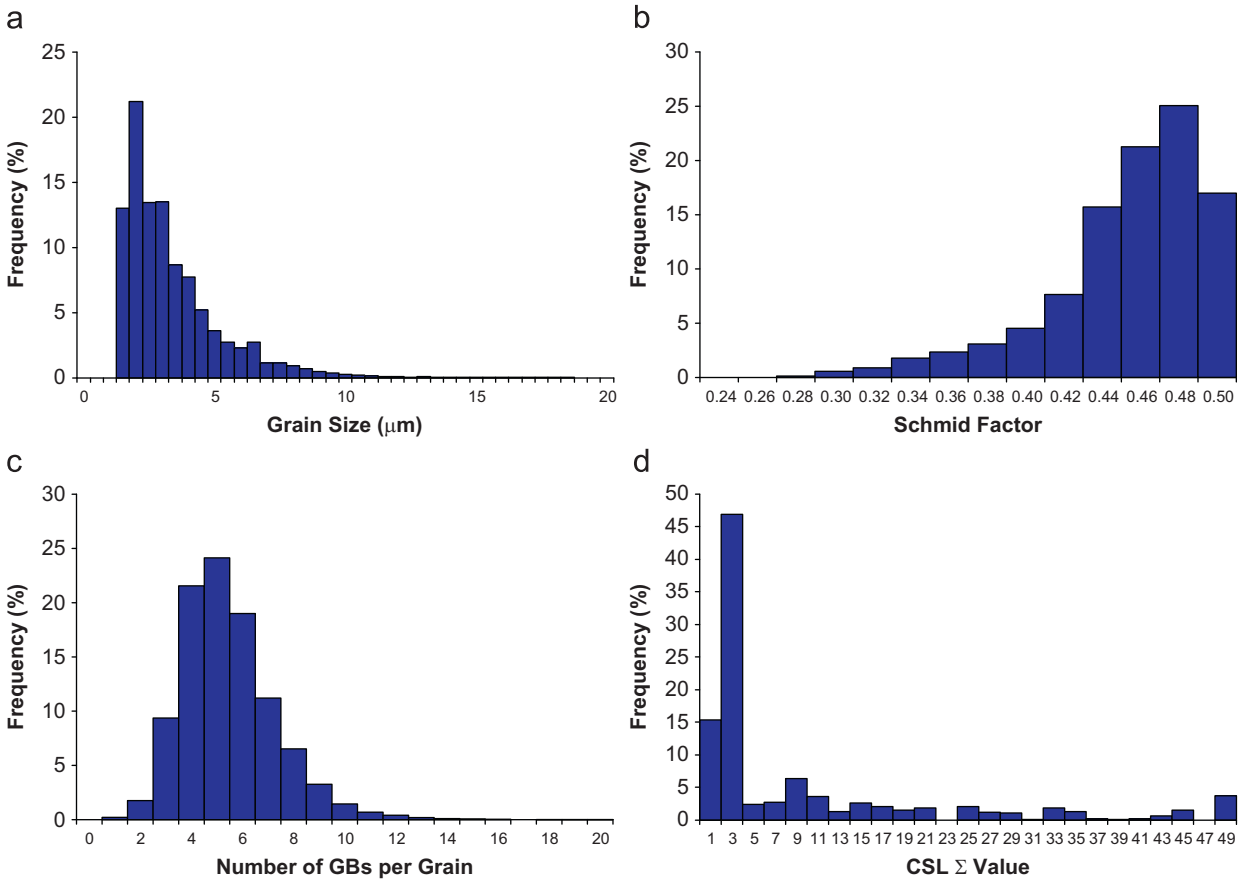

Fig. 2. By pooling the EBSD results from three specimens, histograms are calculated of the: (a) grain size, (b) Schmid factor, (c) number of GBs per grain for a two dimensional cross-section of the grain, and (d) GB character in terms of the CSL Σ values.

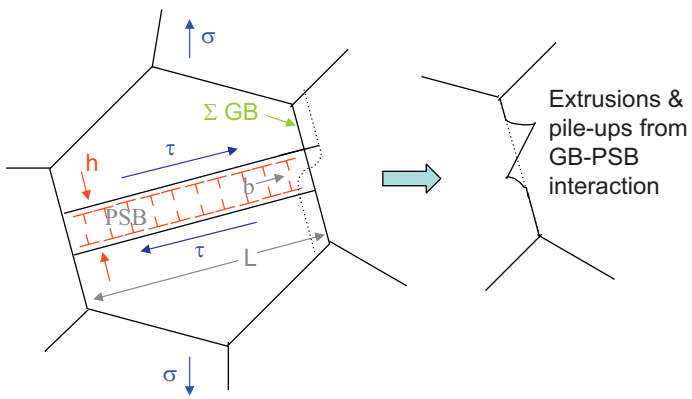

Fig. 3. Schematic of the PSB geometry in the polycrystal. The PSB forms across a grain of size L and orientation (Schmid factor, m) and intersects a pair of GBs each with an associated Σ value. The PSB interaction with GBs leads to static extrusions across the GB in the form of ledges and steps.

cases, where the PSB cannot traverse the GB, the dislocations are blocked from transmitting into the adjacent grain and pile-up at the GB. This ultimately results in stress concentration and the formation of a static extrusion or ledges/steps, as shown in Fig. 3, thus roughening the GB and likely initiating a crack.

It has been shown experimentally that PSBs can penetrate low-angle GBs (LAGBs) (Kobayashi et al., 2009; Zhang and Wang, 2000, 2003; Zhang et al., 2003, 1998), consequentially PSBs can form over multiple grains. LAGBs are defined as a misorientation between grains of less than 15°, also referred to, in literature, as a $\Sigma 1$ GB according to the coincidental site lattice (CSL) (Grimmer et al., 1974; Kronberg and Wilson, 1949) theory using the Brandon condition (Brandon, 1966).

From our EBSD analysis, the LAGBs are identified within the material (Sangid et al., 2010). In these cases, the PSB is permitted to traverse the LAGB and into the adjacent grain. PSB transmission across GBs is observed for this material (U720), as shown in Fig. 1c. This can occur multiple times if LAGB connect grains adjacent to one another, in such cases the Schmid factors are averaged and the grain areas are summed to determine the attributes of the cluster from the individual grains.

3. Energy approach and balance

As previously mentioned, the PSB–GB interaction governs the fatigue life in polycrystals. Our approach is to model the energy of a persistent slip band structure, E, and use its stability with respect to dislocation motion as our failure criterion for fatigue crack initiation within the bulk of a polycrystalline material. This approach allows us to address the small-length scale problems via incorporation of atomistic simulations. Many of the details of this model can be found in Appendix A and Sangid et al. (2011b), although a broad overview of the governing equations is given in this section. Hence, the atomistic simulations provide important insights into the energy barriers and physics of the GBs, which are crucial to fatigue of a polycrystalline material. All the contributing energy factors to the PSB are addressed in our energy balance:

$$E = -E^{\sigma}_{app}(\sigma,m,h,L,N) - E_{hard}(\rho,h,L,N) + E^{disl}_{pile\text{-}up}(h,d,L,N) + E^{disl}_{nuc}(m,\rho,\Sigma,h,L,L',N) + E^{PSB-GB}_{interaction}(m,\Sigma,h,L,L',N) + E^{PSB-GB}_{LAGB}(m,\Sigma,h,L,L',N) + E_{APB}(h,L,\gamma'_{dist},N) + E_{\gamma-SF}(h,L,\gamma'_{dist},N) \quad (1)$$

where σ is the applied stress during fatigue loading, N is the number of cycles, m is the Schmid factor of the grain containing the PSB, L is the grain size, L' is the grain size of the neighboring grains, h is the height of the PSB, d is the distance between PSB walls, ρ is the dislocation density within the PSB, Σ is the character of GB in the CSL model, and γ' is the distribution of Ni_3Al precipitates (in terms of volume fraction, f). The first three terms of the energy expression displays terms that are associated with the continuum length scale, and other terms are derived by atomistic simulations. Each term is discussed in the subsequent sections.

3.1. Continuum stress field terms

The continuum terms (first three terms in Eq. (1)) create an internal stress field, E_{τ}; the glissile dislocations must overcome this stress field to plastically deform the material (Eshelby et al., 1951) by an increment of slip, ∂X_i, as follows:

$$E_{\tau} = -E^{\sigma}_{app} - E_{hard} + E^{disl}_{pile\text{-}up} + E^{disl}_{nuc} = \sum_i \overline{\tau}\,\vec{b}\,Ln^{layers}\partial X_i \quad (2)$$

where the overall shear stress, $\overline{\tau}$, is composed of the contribution from the dislocation field in the PSB structure, τ^{dis}, the work-hardening of the system, τ^{h}, and the external applied resolved shear stress, τ^{A}. In this equation, the Burgers vector of the dislocations and number of moving planes within the PSB are denoted by $\boldsymbol{b}$ and n^{layers}, respectively.

$$\overline{\tau} = \tau^{dis} - \tau^{h} - \tau^{A} \quad (3)$$

The concepts of superposition of the stress fields (including external applied stresses and dislocation–dislocation interactions) on the movement of dislocations have a long standing foundation in continuum mechanics modeling (Sofronis and Birnbaum, 1995). Each of these terms is described in detail in Appendix A.

3.2. Atomistic contributions

During the fatigue process, dislocations nucleate and shear the γ' precipitates to form slip bands. Once formed, the dislocations within the PSB interact with the GB. In order to capture the physics at the grain boundary interface, it is necessary to investigate this problem at a smaller scale. Hence, atomistic simulations in the form of molecular dynamics (MD) were utilized and the results are incorporated into the energy balance in the form of energy barriers. As previously mentioned, the GBs within the microstructure of U720 were characterized by EBSD and the corresponding energies were measured from MD, as shown in Fig. 4a (Sangid et al., 2010). The following addresses the five last terms in Eq. (1).

Dislocations nucleate during fatigue loading and agglomerate in the PSB resulting in a hardening response. GBs act as distinct sources for dislocations. Depending on the character of each GB, there is a different energy barrier for dislocation nucleation from the GB. In Appendix B and (Sangid et al., 2011a), it is shown that the energy barrier for nucleation, $E^{\gamma-nuc-GB}_{MD}$, is inversely related to the static GB energy, E^{GB}_{Static}, through a power law relation (Fig. 4b):

$$E^{\gamma-nuc-GB}_{MD} = 6.0 \times 10^{15}(E^{GB}_{Static})^{-1.3} \quad (4)$$

Additionally, dislocation evolution is seen within each grain in the cluster. Hence, the energy associated with dislocations nucleating and agglomerating within the PSB is taken from the most favorable GB to emit dislocations during loading. In other words, as shown in Fig. 4b, the lowest energy barrier for nucleation is analogous to the highest static GB energy, which is the GB most likely to emit dislocations within each grain of the cluster. This highest GB energy value per grain is weighted by the grain area and summed for each grain within the cluster. With this information, we can

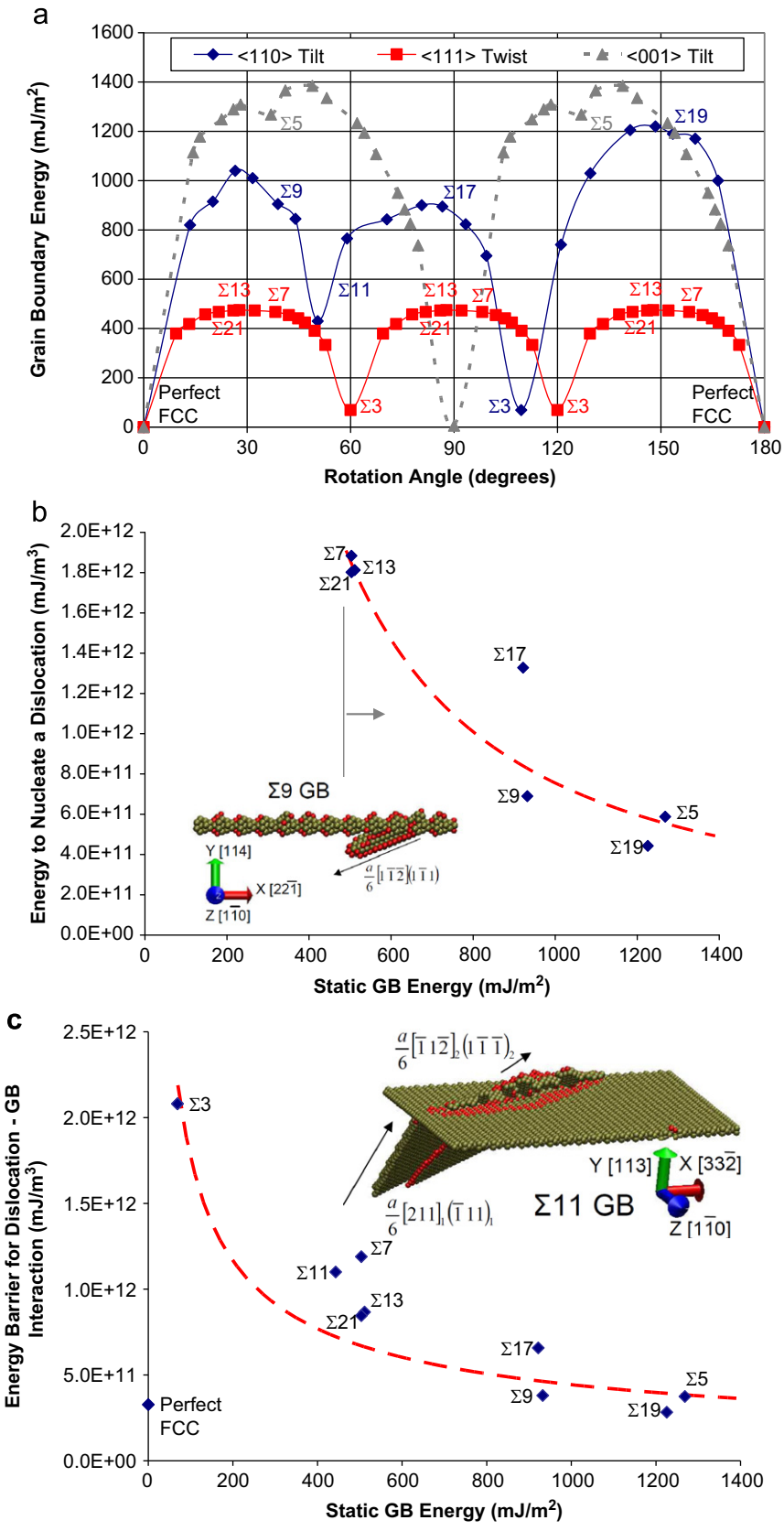

Fig. 4. (a) The grain boundary energy shown as a function of the rotation angle for nickel in the ⟨1 1 0⟩ tilt, ⟨1 1 1⟩ twist, and ⟨0 0 1⟩ tilt directions. (b) Energy barriers for slip to nucleate from a GB plotted against the static GB energy for various types of Σ CSL value GBs. The data range is only valid to the right of the gray solid line, since dislocations did not nucleate at the GB in cases of low GB energy in the MD simulation. (c) Energy barriers for slip to penetrate a GB plotted against the static GB energy. In each plot, there is a relationship between the static GB energy and GB energy barrier as shown by the power law fit of the data (red dash line). (For interpretation of the references to color in this figure legend, the reader is referred to the web version of this article.)

model the energy associated with the nucleation of dislocations for a cluster containing j grains as

$$E_{nuc}^{disl} = \sum_i \partial X_i \left\{ \sum_j E_{MD,j}^{\gamma-nuc-GB} L_j^2 \right\} (\rho - \rho_o) \vec{b}\, h \tag{5}$$

The number of dislocations nucleating within the PSB during loading is represented by the evolution of dislocation density within the PSB multiplied by the cross-sectional area of the PSB: $(\rho-\rho_o)hL$. This energy contribution is dependent on the individual slip increment, ∂X_i for movement of a dislocation after nucleation.

As previously mentioned, dislocations glide within the PSB and as a result the dislocations interact with the GB. Depending on the character of the GB, there are different energy barriers for dislocations to penetrate the GB. Once again, this value is specific to the CSL Σ value, as measured from MD simulation (Appendix B), as shown in Fig. 4c. The relationship between the energy barriers for a dislocation to penetrate the GB, $E_{MD}^{\gamma-slip-GB}$, and the static GB energy is given by

$$E_{MD}^{\gamma-slip-GB} = 2.8 \times 10^{13} (E_{Static}^{GB})^{-0.6} \tag{6}$$

In cases where the dislocations traverse the GB, the PSB forms a static extrusion at the GB, as shown in Fig. 3. The intersection between the PSB and GB is a preferred site for crack initiation (Sangid et al., in press). Thus, we must account for the energy in the formation of a static extrusion at the GB of the polycrystal; hence the associated energy with the PSB–GB interaction resulting in dislocation pile-ups and step/ledge features at the GB is given by

$$E_{interaction}^{PSB-GB} = \sum_i \partial X_i E_{MD}^{\gamma-slip-GB} n_{dis}^{pen} \vec{b}\, h, \tag{7}$$

where n_{dis}^{pen} is the number of dislocations that penetrate the GB (Appendix A). The GB with the largest energy barrier analogous to the lowest static GB energy (according to Fig. 4c) is selected for the grains at the outskirts of the grain cluster; this value is used in Eq. (7) to account for PSB–GB interactions. Additionally, the energy of the PSB traversing the LAGB, $E_{LAGB}^{\gamma-slip-GB}$, is accounted for in a similar manner:

$$E_{LAGB}^{PSB-GB} = \sum_i \partial X_i E_{MD}^{\gamma-slip-GB} \vec{b}\, h, \tag{8}$$

where $E_{MD}^{\gamma-slip-GB}$ is the energy barrier for slip penetration into the adjacent grain as indicated in Fig. 4c for a $\Sigma 1$ GB.

Finally, slip bands form in the material by cutting through the γ matrix and the γ' precipitates. In order to do so, the dislocation must overcome an associated energy based on the glissile dislocation destroying the (FCC) lattice stacking sequence in the γ matrix and stacking sequence and order in the γ' precipitates, which correspond to the stacking fault, γ_{SF}, and anti-phase boundary, γ_{APB} (APB) energy, respectively. The γ' precipitates are composed of Ni_3Al-type in an ordered $L1_2$ structure, thus the ordering of the Ni and Al atoms within the lattice creates the additional obstacle to slip. Hence, the energy associated with the formation of the PSB from shearing the γ matrix and the γ' precipitates is given by

$$E_{APB} + E_{\gamma-SF} = \left(f \int_o^L \gamma_{APB}\, dL + (1-f) \int_o^L \gamma_{SF}\, dL \right) n_{eff}^{layers} \partial X, \tag{9}$$

where f is the volume fraction of γ' precipitates and n_{eff}^{layers} is the number of effective layers contributing to the stacking fault or APB energy, as each additional layer provides 95% of the energy value of the prior layer. For U720, the fraction of γ' precipitates is approximately 0.20, which was determined by the use of image analysis software on optical micrographs.

3.3. Failure criterion

Remaining consistent with the other historical energy balances for fracture (Griffith, 1920), twins (Cooper, 1965, 1966), dislocation emission (Rice, 1992; Rice and Thomson, 1974), and crack initiation (Tanaka and Mura, 1981), we check the stability of the PSB by differentiating with respect to plastic deformation, specifically movement of the glissile dislocations. Each component of the energy balance in Eq. (1) is expressed as an increment of slip, ∂X_i, thus making differentiation very amenable and computationally efficient. The minimum energy of the PSB is determined:

$$\frac{\partial E}{\partial X_i} = 0. \tag{10}$$

Additionally, the second derivative of the energy must be positive to ensure that the energy corresponds to a local stable minimum. Thus, we establish Eq. (10) as our failure criterion for fatigue crack initiation corresponding to stability and equilibrium of the PSB's energy.

Hence, this model sums the energy contributions of each term in Eq. (1) within the grain or grain cluster most likely to form a PSB (favorable energy for failure based on combination of orientation, grain size, and grain boundary character—CSL Σ values). This energy balance evolves with increasing loading cycles; meanwhile physically there is significant irreversible slip within the PSB leading to dislocations penetrating the GB thereby forming extrusions. When stability of the PSB and a minimum energy configuration is achieved, a crack initiates from the PSB. The crack nucleates at the site of the static extrusions (ledge and step features), i.e. PSB–GB intersection.

4. Establishing simulated microstructures

Thus far, we have presented a methodology for predicting fatigue crack initiation based on an energy balance, which exams each grain in the polycrystalline aggregate along with the formation of clusters, i.e. grains connected by LAGBs. We assume a PSB exists in every grain and grain cluster and negate PSB–PSB interactions. For each PSB, we perform our energy balance and check for stability for each grain and cluster of grains, and thus we can identify which PSB results in the (lowest) limiting life in terms of number of applied loading cycles. In doing so, we can predict the location in the microstructure that is most susceptible to fatigue crack initiation and the resulting life of the polycrystalline aggregate. In a sense, a weakest link is determined and cracks initiate from the PSB–GB interaction in this grain or grain cluster. From this methodology, fatigue life is tied to the energy of a critical PSB, which inherently accounts for the microstructure of the material. By varying the microstructure, we can account for microstructurally driven fatigue scatter.

As previously mentioned, the attributes associated with the microstructure of the material were measured from EBSD scans of three specimens and pooled together to establish representative distributions. The measured attributes are the grain size, grain orientation in terms of Schmid factor, number of adjacent grains, and CSL Σ value as shown in Fig. 2. In Fig. 2d, the character of the GBs are consolidated by the CSL Σ value, although in actuality we measure an axis/angle pair for each GB, which provides a more accurate representation of the boundary. Using the axis/angle description, we calculate the associated GB energy from MD simulations (Sangid et al., 2010). Hence, an aggregate of 2000 grains was constructed, and for each grain, the grain size, grain orientation (Schmid factor), and number of GBs were selected randomly from the measured distributions (Fig. 2a–c, respectively). Also, the neighbor information for each grain is randomly assigned and the GB character in terms of an axis/angle pair and its static interfacial energy is allocated from the measured distribution (Fig. 2d) for the GB connecting the two adjacent grains in a self-consistent manner.

Thus, attributes are randomly assigned for each grain in the polycrystal to create a 'simulated specimen', as shown in Fig. 5. We repeat this process to generate 1000 specimens, which accounts for the variability in the material based within the observed ranges of microstructural features. For each specimen, the microstructure is simulated, grains/clusters most likely to fail are identified, and the cycles to crack initiation is predicted for a series of six applied strain ranges. Hence, the aforementioned code takes $\sim$28.2 s to run for each specimen on a standard desktop computer, thus offering substantial computational savings as opposed to other microstructurally driven fatigue software.

5. Results and discussion

For each of the 1000 simulated specimens, the fatigue life in terms of cycles to crack initiation is predicted using the methodology outlined in Section 3. The results are shown in Fig. 6 (1000 model predictions—red diamonds compared to 84 experiments—blue triangles) and Table 1. Based on these results, we can conclude that by varying the microstructure, the model accurately accounts for the fatigue scatter. For each strain range, the averages of the predicted results and experiments are nearly identical, further the minimum and maximum values are in good agreement.

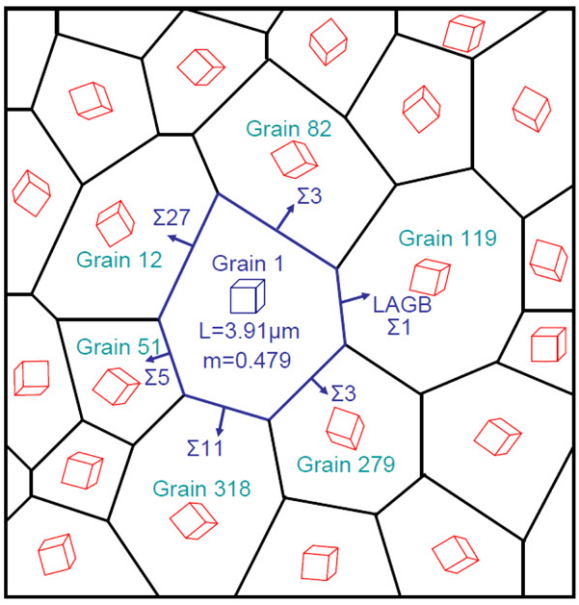

Fig. 5. Schematic of a reconstructed microstructure for a simulated specimen. For each grain, the size, orientation, number of GBs, and associated GB character is selected randomly from the distributions in Fig. 2; afterwards, the nearest neighbors are assigned.

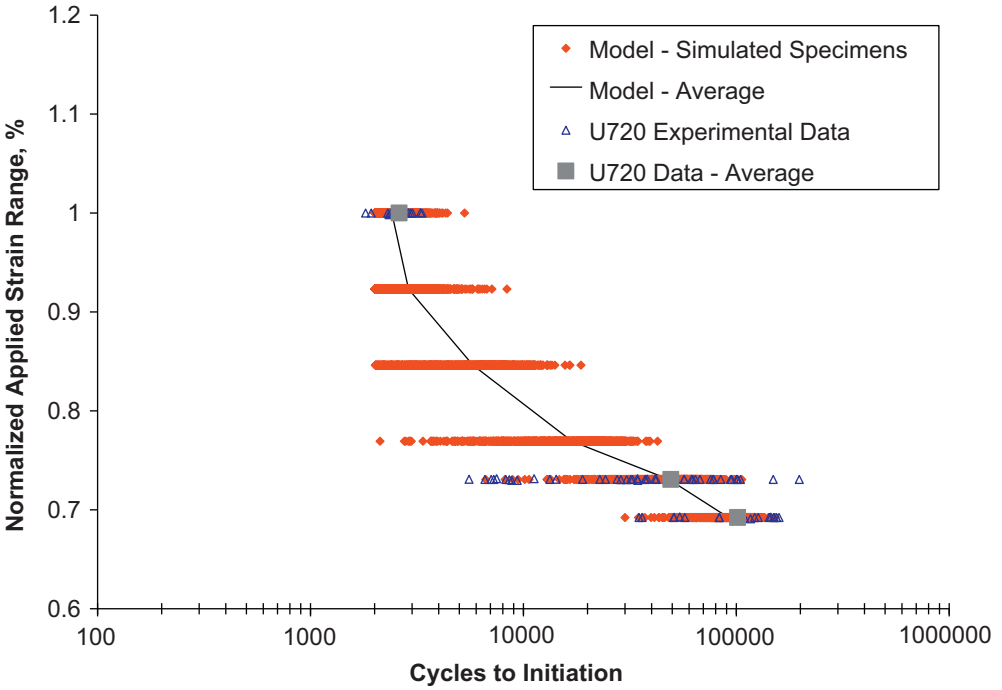

Fig. 6. Predicted fatigue results for 1000 simulated specimens at each strain range compared to specimen from 84 fatigue experiments. The individual specimens as well as the averages provide good agreement between model predictions and experimental results. Please note that the applied strain ranges are normalized values.

Table 1
Model predicted fatigue results in terms of number of cycles until crack initiation for 1000 simulated specimens at a series of normalized applied strain ranges.

Strain range	Average	Standard deviation	Log average	Log standard deviation	Maximum	Minimum	Number of data points
1.00	2410	419	2379	342	5297	2003	1000
0.92	2886	812	2792	615	8372	2003	1000
0.85	5794	2674	5193	1974	18,616	2018	1000
0.77	16,914	7097	15,178	5981	42,667	2121	1000
0.73	48,348	17,034	44,889	15,108	105,980	6654	1000
0.69	91,861	20,447	89,367	19,248	152,630	30,024	1000

Within a given specimen, the grain cluster most likely to fail is dependent on the applied strain range. In other words, based on the loading magnitude, we see different terms dominate the energy balance (Eq. (1)) resulting in crack initiation occurring in a different combination of microstructure features. Hence, for the 1000 simulated specimens, modeled at six applied strain ranges, we have 6000 possible failure locations from individual grains or grain clusters, which allows us to analyze the statistics of the predicted locations likely to initiate cracks.

The vast majority (96%) of the cracks initiate due to PSB interaction with a twin boundary, as shown in Fig. 7a, which is in agreement with experimental observations (Boettner et al., 1964; Guo et al., 2005; Hashimoto et al., 1999; Llanes and Laird, 1992; Miao et al., 2009; Qu et al., 2008; Thompson, 1972) and Fig. 1a,b as twins are evident within the facets. As shown in Fig. 4c, the $\Sigma 3$ twin boundary exhibits the highest energy barrier for slip transmission. Thus, dislocation motion is impeded by twins resulting in pile-ups. To alleviate the high energy and stress concentration caused by the pile-ups, the material forms a crack in the vicinity of the twin. Hence, we experience cracking near twin boundaries in our simulations, as a consequence of the high associated energy barrier coupled with the large percentage of annealing twins within this material (Fig. 2d). Additionally, the PSB preceding crack initiation occurs in a single large grain 55% of the time as shown in Fig. 7b. In the remaining simulations, PSBs spanning multiple adjacent grains connected by LAGBs initiate cracks, although these grain clusters are most likely to be comprised of only two (30.9%) or three (10.9%) grains. Seven grains constituted the largest predicted cluster, albeit this was an isolated and rare case.

Further, the sizes of the simulated grain clusters initiating cracks are analyzed and compared with the experimental distributions of grain size and facet size, as shown in Fig. 8. We see the size of the problematic grain clusters is in the range of 7.7–21.2 μm. Hence, this range is on the tail end of the measured grain size. Thus, in the cases where the grain cluster is

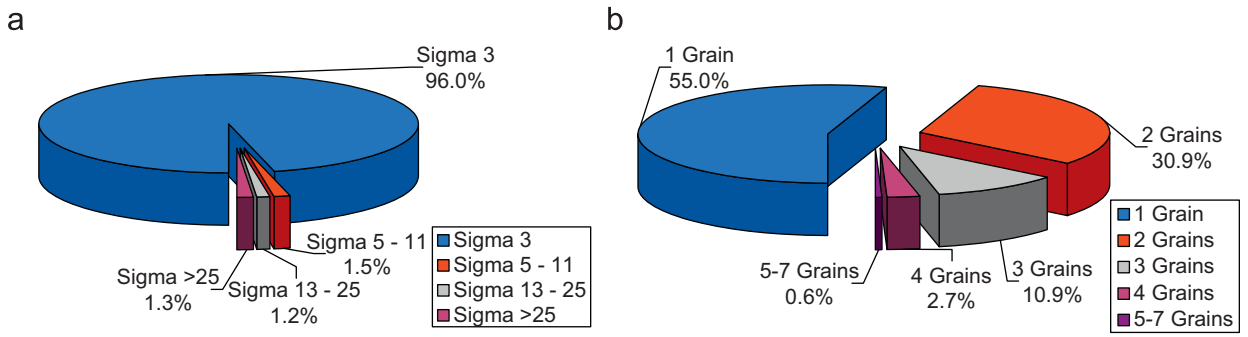

Fig. 7. From the 1000 simulated specimens at each strain range, the grain cluster, in which a crack was predicted to initiate, is analyzed. (a) Cracks initiated due to PSB–GB interaction, thus the distribution of GB Σ character resulting in crack formation is shown. As expected, the model predicts that most cracks initiate in the vicinity of $\Sigma 3$ GBs, i.e. twins. (b) The distribution of number of grains within the grain cluster most likely to fail.

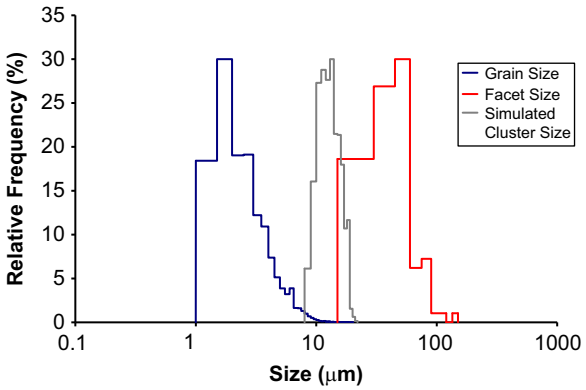

Fig. 8. Histogram comparisons for the grain size measured from EBSD on the three pooled specimens, the facet size measured from SEM images of 89 failed fatigue specimens, and the size of the simulated grain cluster most likely to initiate a crack from a PSB.

comprised of a single grain (55%), these grains are amongst the largest size in the measured population. Also, the cluster size distribution approaches the facet sizes (15–135 μm) measured from the fracture surfaces of 89 failed fatigue experiments. We would expect to see larger grain clusters, which mimic the facet size, if the EBSD scans encompassed a greater area or the simulated specimens contain a greater number of grains. Another possible reason for the discrepancy between cluster size and facet size is that experimentally short cracks initiate and experience slow crack growth. These fine growth features cannot be distinguished in the facet; hence, the facet is not a good measure of grain cluster size as a precursor to crack initiation.

As previously discussed, many contributing microstructural variables (i.e. grain orientation, grain size, GB character, γ' precipitate density, and neighboring grains) affect the predicted fatigue life. We investigated the correlation between each of these parameters to the predicted fatigue life; the results showed that the grain size dependency is best correlated to the fatigue life. As shown in Fig. 9, for each of the 1000 simulated specimens (at 0.73% applied strain), the predicted fatigue life is shown as a function of the size of the grain or cluster of grains most likely to initiate a crack. When the microstructure's weakest link is composed of a larger grain, a shorter fatigue life is observed. The data is split into three categories, single grain failures (55%), clusters consisting of two grains (30.9%), and clusters consisting of three or more grains (14.1%). From these data sets, a regression analysis was performed. On average, clusters composed of a greater number of grains have a shorter fatigue life for a given cluster size. Of course, the data does not collapse to a single line since many other factors play a role in predicting fatigue life. Further, in Fig. 9, the gray dashed line represents the minimum predicted fatigue life based on the critical grain size within the distribution. This type of curve can be used for design purposes as microstructures are typically inspected for ALA (as large as) grains. The fatigue life can be simply forecasted from this curve in a conservative manner (since these ALA grains are not necessarily the weakest link), while more accurate predictions can be determined when factoring in the other microstructural parameters into the fatigue model.

In essence, this model identifies the weakest link in the microstructure, which ultimately results in crack nucleation. The nature of weakest link models is that with increased sampling of grains, the probability of finding a detrimental grain cluster increases. Changing the representative volume element (RVE, i.e. number of grains in our simulated microstructure) results in a shift of the predicted fatigue response, thus displaying lower lives, as shown in Fig. 10 for

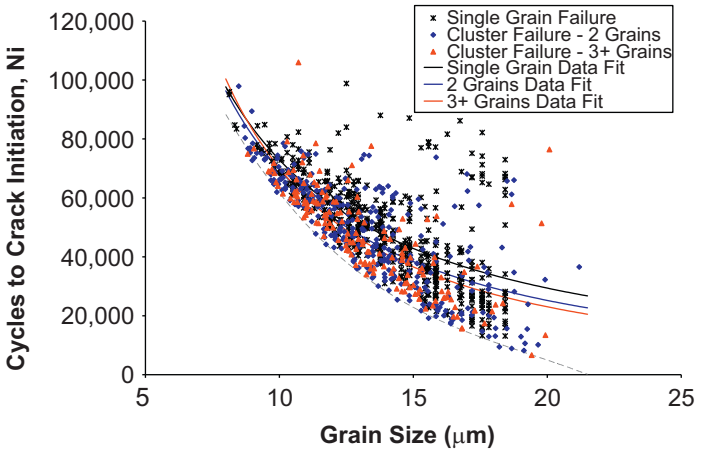

Fig. 9. Results of 1000 simulated specimens at 0.73% (normalized) applied total strain range. The predicted fatigue life is plotted against the size of the individual grain or cluster of grains most likely to initiate a crack in each simulated specimen. The data is separated into the number of grains causing failure and best fit lines are drawn for each group. If a single grain causes failure, the *x*-axis refers to the size of that specific grain; if multiple grains cause failure, the *x*-axis refers to the size of that specific grain cluster resulting in crack initiation. The dashed gray line represents the minimum fatigue life for a given grain size, which may be used for design purposes.

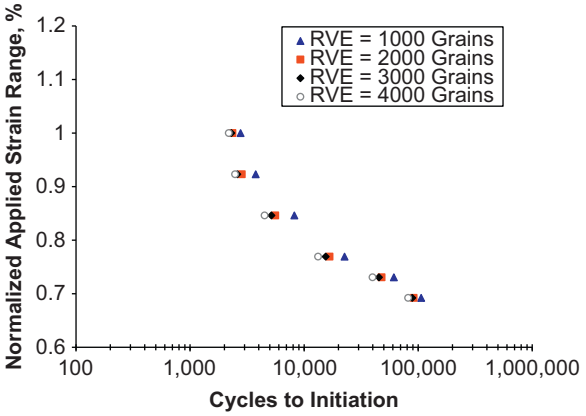

Fig. 10. Predicted fatigue results in terms of average life for 100 specimens. This plot displays the effect of the number of grains within the simulated microstructure, i.e. representative volume element, on the predicted values of cycles to initiation. As expected, more grains increases the probability of finding a weakest link and early failure. Please note that the applied strain ranges are normalized values.

100 simulated specimens at each RVE size: 1000, 2000, 3000, and 4000. In other words, by increasing the number of grains or RVE, we increase the probability of finding a larger weakest link in the microstructure and effectively lower the fatigue life of the simulated specimen. Of course, the RVE size is a function of the microstructure, which in the present case is characterized by EBSD scans of 3 specimens containing (2373, 3664, and 7424 grains). Therefore, our pooled distributions are comprised of 13,461 grains, hence choosing a RVE size of 2000 grains represent a substantial subset of each EBSD scan, while still addressing computational efficiency.

In general, fatigue modeling, especially in the presence of scatter, has not been based on a physics of solids approach. Hence the present study addresses this need as a model is developed based on the microstructure of the material. Our model displays excellent agreement between predicted fatigue scatter and experimental results; thus, providing a powerful tool demonstrating predictive capabilities.

6. Conclusions

This study represents a substantial effort in the field of physically based fatigue modeling. The major contributions are as follows:

- A methodology was introduced to establish an energy balance for a PSB, which evolved with increase in fatigue cycles. The energy balance includes terms from the continuum scale to calculate the stress fields and the atomistic scale to

account for slip interactions with GBs and precipitates. Stability of the PSB occurs at a minimum value of its energy, which was computed as the derivative of the total PSB energy with respect to plastic deformation (i.e. an increment of slip) reaching zero, corresponding to our failure criterion and crack initiation. This methodology is attractive since it is physically based and inherently accounts for the microstructure of the material. Hence, the most probable sites for PSB formation and failure within the microstructure are identified and monitored.

- EBSD scans were completed on three specimens and pooled together to obtain distributions of the representative grain size, orientation (Schmid factor), number of adjacent grains, and GB character in terms of an axis/angle pair with a corresponding GB energy. From this data, simulated microstructures were generated by randomly assigning attributes to the grains from the measured distributions. Using our fatigue analysis software, the fatigue life was predicted on each of these simulated specimens and compared with experimental results, which displayed excellent agreement both in terms of scatter and average values.
- From the thousands of simulated specimens, we can conclude that single large grains are most likely to form cracks. Although two or three grains connected by LAGBs were a significant source of crack initiation; also in one rare case, a crack initiated from a grain cluster comprised of seven grains.
- In nearly all the simulated specimens, the cracks initiated near a twin boundary, corresponding to the experimental observations. This is established in our model as twin boundaries possess the highest energy barrier for slip transmission. Thus, the PSB–GB interactions resulted in dislocation pile-up, stress concentration, an increase in energy, and crack initiation.

Acknowledgments

Support for this work was provided primarily by Rolls-Royce Corporation and partially by the National Science Foundation, DMR 08-03270. The authors would like to thank David Furrer and Jeffrey Stillinger from Rolls-Royce Corporation for discussions on fatigue scatter.

Appendix A. Additional details regarding terms in Fatigue Model

In Eq. (1), dislocations glide within the PSB; in order to account for this energy, it is paramount to account for each layer of successive glissile dislocations. The number of moving planes within the PSB is quantified by n^{layers}, which is related to the PSB width, h:

$$n^{layers} = h/y^e \tag{A.1}$$

The width of the PSB, h, was measured from the TEM images of U720 (e.g. Fig. 1d) and must be normalized by the distance between dislocations within the PSB to find the number of layers, y^e (Essmann and Mughrabi, 1979). The evolution of the width of the PSB, h, is shown in Fig. 11a, which we have measured experimentally using TEM analysis; through this analysis, we calculate evolution of n^{layers} in the PSB. The individual stress components that contribute to the internal stress field are discussed next.

Within the PSB, dislocations agglomerate into walls and form dipole structures, in order to minimize their total energy, which is modeled as layers of opposing signed dislocations (Essmann et al., 1981; Tanaka and Mura, 1981) separated by a distance, h. Within each layer is a series of dislocations, equally spaced by d. In doing so, we can assume linear elastic, isotropic, plane strain behavior thus greatly simplifying the problem, in order to find the stress within the PSB. The stress field created by the dislocation dipoles within the PSB is given by τ^{dis} as it varies spatially (x,y) within the PSB (Brinckmann, 2005):

$$\tau^{dis} = \frac{\mu b\pi}{(1-\nu)d^2}\left(\frac{y(1-\cos(2\pi x/d)\cosh(2\pi y/d))}{(-\cos(2\pi x/d)+\cosh(2\pi y/d))^2} - \frac{(h+y)(1-\cos(2\pi x/d)\cosh(2\pi(h+y)/d))}{(-\cos(2\pi x/d)+\cosh(2\pi(h+y)/d))^2}\right) \tag{A.2}$$

where the elastic constants μ, ν are the shear modulus and Poisson ratio at elevated temperatures, respectively. The spacing between dislocation walls, d, is determined based on the dislocation density within the PSB, ρ, as follows:

$$d = \frac{1}{\sqrt{\rho}} \tag{A.3}$$

The work-hardening of the forest dislocations within the PSB is assumed to follow a Taylor relationship:

$$\tau^h = \alpha\mu b\sqrt{\rho} + \tau_o \tag{A.4}$$

where the scalar, α=0.45 (Argon, 2008). The initial shear stress, τ_o:

$$\tau_o = \frac{\sigma_y}{M} \tag{A.5}$$

is given by the yield stress at the test temperature normalized by the Taylor factor, M, which is 3.06 (random orientation) for this material. The evolution of dislocation density with loading cycles (N) was extracted from literature for a similar

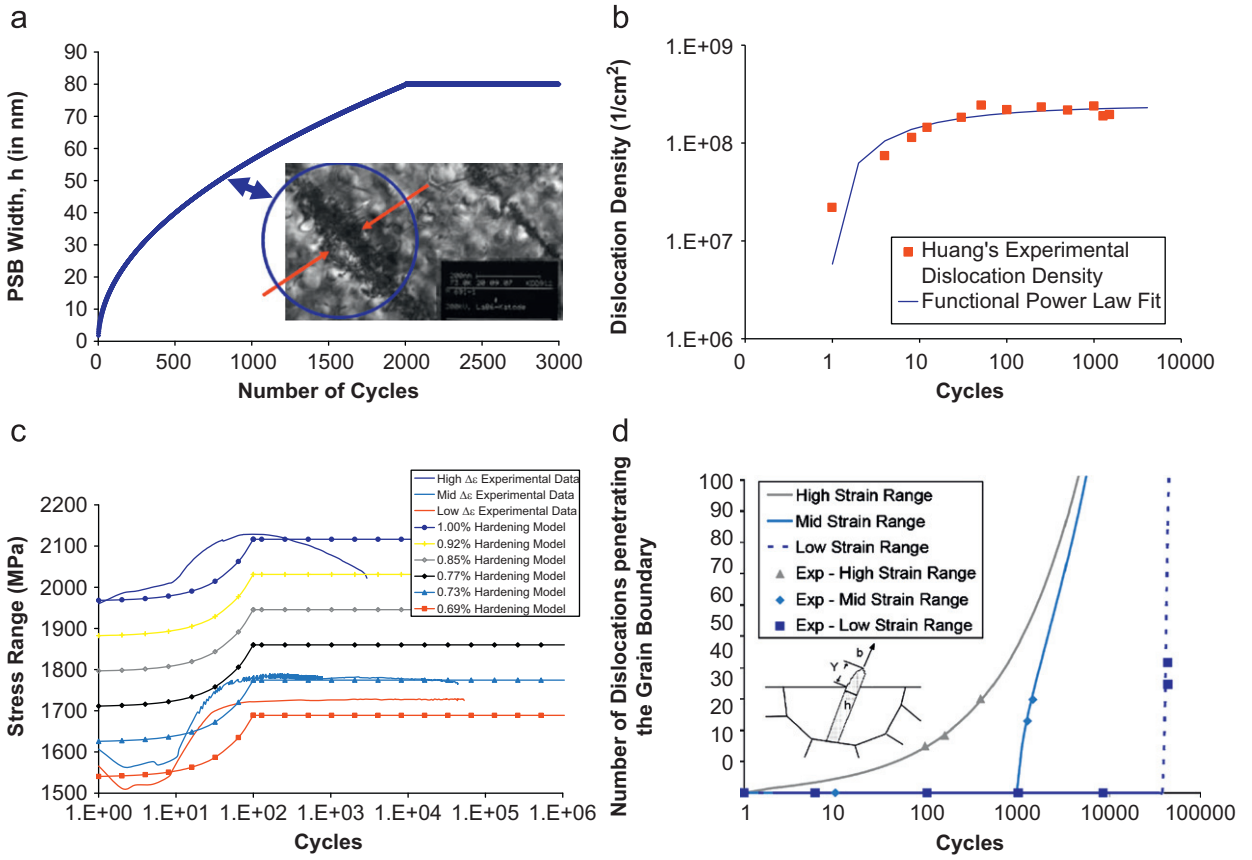

Fig. 11. Experimentally based functional fits used in the model. (a) PSB width, h, evolution during cyclic loading. The saturation is measured from TEM analysis. (b) A power law fit is used to fit the dislocation density evolution. This data is taken from literature for a nickel-based superalloy from Huang et al. (2010). (c) Evolution of the stress response to a strain-controlled LCF experiment, where each $\Delta\varepsilon$ value is normalized. At the highest strain range, multiple cracks form and interact resulting in cyclic softening towards failure. (d) Number of dislocations forming an extrusion during cyclic loading. The data is measured via AFM by Risbet and Feaugas (2008) and Risbet et al. (2003, 2009) for a nickel-based superalloy and a functional was fit to the data according to Eq. (A.12).

Ni-based superalloy studied by Huang et al. (2008), and a power law was used to fit the data, $F(N)$:

$$F(N) = A_1 N^{c_1} + A_2 \tag{A.6}$$

The experimental data and regression of the dislocation density evolution are shown in Fig. 11b. Since Huang's study only represents one test condition, the functional form of the dislocation density was amended by the following ratios for each variable:

$$\rho \propto \frac{(\gamma^{pl}_{ratio})^2 (m_{ratio})^2}{\exp(E^{\dot{\gamma}-nuc-GB}_{ratio})} F(N) \tag{A.7}$$

The relationship for the Schmid factor, m, and dislocation density is derived from simple expressions for the Taylor hardening and inelastic strain rate, respectively.

$$\tau = m\sigma = \alpha\mu b\sqrt{\rho} \Rightarrow \rho \propto m^2 \tag{A.8}$$

Similarly, by relating the Orowan equation to the inelastic strain rate, an expression between the dislocation density and activation energy is developed.

$$\dot{\gamma} = \vec{b}\,\rho\overline{v} = \dot{\gamma}_o \exp\left(\frac{-\Delta E}{kT}\right) \Rightarrow \rho \propto \exp(-\Delta E) \tag{A.9}$$

Due to the volatile nature of the exponential term, a Taylor expansion was used to the second power. The plastic strain amplitude relationship was verified by experimental data by Grosskreutz (1971) for the dislocation density in copper single crystals as a function of shear flow stress, which can be related to the plastic shear strain as follows:

$$\rho \propto (\gamma^{pl})^2 \tag{A.10}$$

The applied shear stress for each grain, τ^A, is measured from the hysteresis behavior of the material during the strain control test and multiplied by the Schmid factor of the individual grain, m.

$$\tau^A = m\Delta\sigma^A = mH(N) \tag{A.11}$$

The evolution of alternating stress during loading, $\Delta\sigma^A$, is obtained from the macroscopic response of the test data for the polycrystalline material, U720, as shown in Fig. 11c. The stress response, $H(N)$, resembles a square root function as it hardens with increasing number of cycles and saturates. The stress is dependent on the applied strain, although at each strain range, the stress saturates after approximately 100 cycles.

In Eq. (7), the number of dislocations that penetrate the GB, n_{dis}^{pen}, can be approximated based on the AFM measurements of extrusions at the surface of a Ni-based superalloy by Risbet and Feaugas (2008) and Risbet et al. (2003, 2009). In their study, they measured the height of the extrusions, which we normalize by the Burgers vector, $\boldsymbol{b}$, to obtain n_{dis}^{pen}. The extrusion height was measured as it evolved with increasing load cycles for various applied strain ranges. After a threshold number of loading cycles, N_{th}, the extrusions appeared and were pronounced; as expected, extrusions are observed after fewer cycles at higher applied strain ranges compared to lower strain ranges. The functional format, $G(N)$, used to fit this data is a square root dependency, based on Mughrabi and Essman's model of surface roughness (Differt et al., 1986; Essmann et al., 1981).

$$G(N) = A_2\sqrt{N-N_{th}} \tag{A.12}$$

Similarly, the experimental data and regression of the number of dislocations that penetrate the GB as a function of applied loading cycles are shown in Fig. 11d. Once again, the values of the AFM measurements must be normalized to account for different microstructure conditions; hence, n_{dis}^{pen} is proportional to the following ratios:

$$n_{dis}^{pen} \propto (\gamma_{ratio}^{pl})^2 (m_{ratio})^2 (L_{ratio}) G(N) \tag{A.13}$$

where the plastic strain ratio is confirmed by the experiments (Risbet et al., 2003) and theory (Mughrabi et al., 1983), and the grain size dependency is derived by modeling the irreversible slip in a PSB (Risbet and Feaugas, 2008). Similar arguments were made for the Schmid factor as aforementioned in Eq. (A.8). More detail on the fatigue model methodology can be found in Sangid et al. (2011b, in press).

Appendix B. MD simulations

MD simulations were created to reconstruct CSL Σ GBs from distinct orientations of crystal lattices consisting of FCC Ni using the Foiles–Hoyt potential (Foiles and Hoyt, 2006). The simulation box was deformed using an NPT ensemble with periodic boundary conditions, where the number of atoms in the simulation box, N, the pressure in the three directions (stress free boundaries), P, and the system temperature, T (10 K), are held constant throughout the simulation. A void was introduced into the system to facilitate dislocation nucleation leading to slip–GB interaction. To grasp the role of the GBs on the energetics of each system, the potential energy of each atom was measured during the simulation. A control box was placed at the intersection of the dislocation and GB along the atoms which play a role in the interaction (selected via the centro-symmetry parameter (Kelchner et al., 1998)); hence, it is not a simple cubic box. Extreme care was taken to select the positions of only the relevant defect atoms to determine the energy upon loading of that atom, which was reduced by the energy of that atom in its static relaxed position and normalized by the volume of the control box. In order to verify these MD calculations for determining the energy barrier, a system was constructed without a GB to mimic slip in an FCC lattice. The result of our MD control box method was compared to the generalized stacking fault energy and produced a modest 6% difference, thus validating this procedure.

This procedure was repeated for various CSL Σ GBs, in order to measure the energy barrier for slip transmission: $\langle 1\,1\,0\rangle$ tilt—Σ3, 9, 11, 17, 19; $\langle 1\,1\,1\rangle$ twist—Σ3, 7, 13, 21; and $\langle 0\,0\,1\rangle$ tilt—Σ5. Similarly, the void was removed from our MD system and the simulation box was deformed to measure the energy barriers associated with slip nucleation from the GB. The Σ3 and Σ11 GBs have a stable configuration, hence nucleation from the GB was not observed in the simulation. We rationalized the energy barriers for various types of GB with their static GB energy. The results of which are shown in Fig. 4b,c as the energy barrier for slip nucleating from a GB and slip transmission across a GB is plotted against the static GB energy for each GB, respectively. There is an inverse relationship between the energy barrier against slip and static energy for each type of GB. A power law function was fit to the data resulting in Eqs. (4) and (6), respectively. Details concerning the methodology of these MD simulations and a discussion of the results can be found in Sangid et al. (2011a).

References

Argon, A.S., 2008. Strengthening Mechanisms in Crystal Plasticity. Oxford University Press.
Boettner, R.C., McEvily, J.A.J., Liu, Y.C., 1964. On formation of fatigue cracks at twin boundaries. Philosophical Magazine 10, 95.
Brandon, D.G., 1966. The structure of high-angle grain boundaries. Acta Metallurgica 14, 1479.
Brinckmann, S., 2005. On the Role of Dislocations on Fatigue Crack Initiation. Zernike Institute for Advanced Materials, University of Groningen, Netherlands.
Cooper, R.E., 1965. The equilibrium shape of deformation twins. Acta Metallurgica 13, 46.

Cooper, R.E., 1966. The equilibrium shape of deformation twins. II. Acta Metallurgica 14, 78.
Differt, K., Essmann, U., Mughrabi, H., 1986. A model of extrusions and intrusions in fatigued metals. II. Surface roughening by random irreversible slip. Philosophical Magazine A (Physics of Condensed Matter, Defects and Mechanical Properties) 54, 237.
Ellyin, F., 1986. Stochastic modelling of crack growth based on damage accumulation. Theoretical and Applied Fracture Mechanics 6, 95.
Eshelby, J.D., Frank, F.C., Nabarro, F.R.N., 1951. The equilibrium of linear arrays of dislocations. Philosophical Magazine 42, 351.
Essmann, U., Gosele, U., Mughrabi, H., 1981. A model of extrusions and intrusions in fatigued metals. I. Point-defect production and the growth of extrusions. Philosophical Magazine A (Physics of Condensed Matter, Defects and Mechanical Properties) 44, 405.
Essmann, U., Mughrabi, H., 1979. Annihilation of dislocations during tensile and cyclic deformation and limits of dislocation densities. Philosophical Magazine A (Physics of Condensed Matter, Defects and Mechanical Properties) 40, 731.
Foiles, S.M., Hoyt, J.J., 2006. Computation of grain boundary stiffness and mobility from boundary fluctuations. Acta Materialia 54, 3351.
Ghonem, H., Provan, J.W., 1980. Micromechanis theory of fatigue crack initiation and propagation. Engineering Fracture Mechanics 13, 963.
Griffith, A.A., 1920. The phenomena of rupture and flow in solids. Royal Society of London—Philosophical Transactions 221, 163.
Grimmer, H., Bollmann, W., Warrington, D.H., 1974. Coincidence-site lattices and complete pattern-shift lattices in cubic crystals. Acta Crystallographica, Section A (Crystal Physics, Diffraction, Theoretical and General Crystallography) A30, 197.
Grison, J., Remy, L., 1997. Fatigue failure probability in a powder metallurgy Ni-base superalloy. Engineering Fracture Mechanics 57, 41.
Grosskreutz, J.C., 1971. The mechanism of metal fatigue. I. Physica Status Solidi B 47, 11.
Guo, X.L., Lu, L., Li, S.X., 2005. Dislocation evolution in twins of cyclically deformed copper. Philosophical Magazine Letters 85, 613.
Hashimoto, S., Ikehata, H., Kato, A., Kato, H., Kaneko, Y., 1999. Fatigue crack nucleation at $\Sigma 3(112)$ boundary in a ferritic stainless steel. Interface Science 7, 159.
Huang, E.W., Barabash, R.I., Clausen, B., Liu, Y.-L., Kai, J.-J., Ice, G.E., Woods, K.P., Liaw, P.K., 2010. Fatigue-induced reversible/irreversible structural-transformations in a Ni-based superalloy. International Journal of Plasticity 26, 1124.
Huang, E.W., Barabash, R.I., Yandong, W., Bj, C., Li, L., Liaw, P.K., Ice, G.E., Yang, R., Hahn, C., Pike, L.M., Klarstrom, D.L., 2008. Plastic behavior of a nickel-based alloy under monotonic-tension and low-cycle-fatigue loading. International Journal of Plasticity 24, 1440.
Jeulin, D., 2001. Random structure models for homogenization and fracture statistics. In: Ostoja-Starzewski, M. (Ed.), Mechanics of Random and Multiscale Microstructures. CISM, pp. 33–92.
Kato, M., Mori, T., 1992. Statistical consideration of fatigue damage accumulation. Mechanics of Materials 13, 155.
Kelchner, C.L., Plimpton, S.J., Hamilton, J.C., 1998. Dislocation nucleation and defect structure during surface indentation. Physical Review B (Condensed Matter) 58, 11085.
Kitamura, T., Ghosn, L.J., Ohtani, R., 1989. Stochastic Modeling of Crack Initiation and Short-Crack Growth under Creep and Creep-Fatigue Conditions. United States, p. 20.
Kobayashi, S., Kamata, A., Watanabe, T., 2009. Roles of grain boundary microstructure in high-cycle fatigue of electrodeposited nanocrystalline Ni–P alloy. Scripta Materialia 61, 1032.
Kronberg, M.L., Wilson, F.H., 1949. Secondary recrystallization in copper. American Institute of Mining and Metallurgical Engineers—Journal of Metals 1, 501.
Kulkarni, S.S., Sun, L., Moran, B., Krishnaswamy, S., Achenbach, J.D., 2006. A probabilistic method to predict fatigue crack initiation. International Journal of Fracture 137, 9.
Llanes, L., Laird, C., 1992. The role of annealing twin boundaries in the cyclic deformation of f.c.c. materials. Materials Science & Engineering A (Structural Materials: Properties, Microstructure and Processing) A157, 21.
Miao, J., Pollock, T.M., Wayne Jones, J., 2009. Crystallographic fatigue crack initiation in nickel-based superalloy Rene 88DT at elevated temperature. Acta Materialia 57, 5964.
Mughrabi, H., Wang, R., Differt, K., Essmann, U., 1983. Fatigue crack initiation by cyclic slip irreversibilities in high-cycle fatigue. ASTM, Dearborn, MI, USA, p. 5.
Pineau, A., 2001. The randomness of fatigue and fracture behavior in metallic materials and mechanical structures. In: Ostoja-Starzewski, M. (Ed.), Mechanics of Random and Multiscale Microstructures. CISM, pp. 163–220.
Przybyla, C.P., McDowell, D.L., 2010. Microstructure-sensitive extreme value probabilities for high cycle fatigue of Ni-base superalloy IN100. International Journal of Plasticity 26, 372.
Qiao, Y., Chakravarthula, S.S., 2005. Effects of randomness of grain boundary resistance on fatigue initiation life. International Journal of Fatigue 27, 1251.
Qu, S., Zhang, P., Wu, S.D., Zang, Q.S., Zhang, Z.F., 2008. Twin boundaries: strong or weak. Scripta Materialia 59, 1131.
Rice, J.R., 1992. Dislocation nucleation from a crack tip: an analysis based on the Peierls concept. Journal of the Mechanics and Physics of Solids 40, 239.
Rice, J.R., Thomson, R., 1974. Ductile versus brittle behaviour of crystals. Philosophical Magazine 29, 73.
Risbet, M., Feaugas, X., 2008. Some comments about fatigue crack initiation in relation to cyclic slip irreversibility. Engineering Fracture Mechanics 75, 3511.
Risbet, M., Feaugas, X., Guillemer-Neel, C., Clavel, M., 2003. Use of atomic force microscopy to quantify slip irreversibility in a nickel-base superalloy. Scripta Materialia 49, 533.
Risbet, M., Feaugas, X., Guillemer-Neel, C., Clavel, M., 2009. Damage in nickel base superalloy: influence of local parameters measured by electron backscattered diffraction and atomic force microscopy. Scripta Materialia 60, 269.
Sangid, M.D., Ezaz, T., Sehitoglu, H., Robertson, I.M., 2011a. Energy of slip transmission and nucleation at grain boundaries. Acta Materialia 59, 283.
Sangid, M.D., Maier, H.J., Sehitoglu, H., 2011b. A physically-based model for prediction of crack initiation from persistent slip bands in polycrystals. Acta Materialia 59, 328.
Sangid, M.D., Maier, H.J., Sehitoglu, H., The role of grain boundaries in fatigue crack initiation - an energy approach. International Journal of Plasticity, in press, doi:10.1016/j.ijplas.2010.09.009.
Sangid, M.D., Sehitoglu, H., Maier, H.J., Niendorf, T., 2010. Grain boundary characterization and energetics of superalloys. Materials Science and Engineering: A 527, 7115.
Socie, D.F., 2005. Probablistic Aspects of Fatigue—Variability. Fracture Control Program, Urbana, IL.
Sofronis, P., Birnbaum, H.K., 1995. Mechanics of the hydrogen-dislocation-impurity interactions. I. Increasing shear modulus. Journal of the Mechanics and Physics of Solids 43, 49.
Suresh, S., 1998. In: Fatigue of Materials 2nd Edition Cambridge Press.
Tanaka, K., Mura, T., 1981. A dislocation model for fatigue crack initiation. Journal of Applied Mechanics 48, 97–103.
Thompson, A.W., 1972. The influence of grain and twin boundaries in fatigue cracking. Acta Metallurgica 20, 1085.
Todinov, M.T., 1998. Probabilistic method for predicting fatigue life controlled by defects. Materials Science and Engineering A A255, 117.
Wirsching, P.H., Torng, T.Y., Martin, W.S., 1991. Advanced fatigue reliability analysis. International Journal of Fatigue 13, 389.
Zhang, Z.F., Wang, Z.G., 2000. Comparison of fatigue cracking possibility along large- and low-angle grain boundaries. Materials Science & Engineering A (Structural Materials: Properties, Microstructure and Processing) A284, 285.
Zhang, Z.F., Wang, Z.G., 2003. Dependence of intergranular fatigue cracking on the interactions of persistent slip bands with grain boundaries. Acta Materialia 51, 347.
Zhang, Z.F., Wang, Z.G., Eckert, J., 2003. What types of grain boundaries can be passed through by persistent slip bands? Journal of Materials Research 18, 1031
Zhang, Z.F., Wang, Z.G., Li, S.X., 1998. Fatigue cracking possibility along grain boundaries and persistent slip bands in copper bicrystals. Fatigue & Fracture of Engineering Materials & Structures 21, 1307.